BIOCHEMISTRY
including biophysical chemistry & molecular biology

Article

pubs.acs.org/biochemistry

# Structure and Function of Non-Native Metal Clusters in Human Arginase I

Edward L. D'Antonio, Yang Hai, and David W. Christianson*

Roy and Diana Vagelos Laboratories, Department of Chemistry, University of Pennsylvania, Philadelphia, Pennsylvania 19104-6323, United States

**ABSTRACT:** Various binuclear metal ion clusters and complexes have been reconstituted in crystalline human arginase I by removing the $Mn^{2+}_2$ cluster of the wild-type enzyme with metal chelators and subsequently soaking the crystalline apoenzyme in buffer solutions containing $NiCl_2$ or $ZnCl_2$. X-ray crystal structures of these metal ion variants are correlated with catalytic activity measurements that reveal differences resulting from metal ion substitution. Additionally, treatment of crystalline $Mn^{2+}_2$-human arginase I with $Zn^{2+}$ reveals for the first time the structural basis for inhibition by $Zn^{2+}$, which forms a carboxylate-histidine-$Zn^{2+}$ triad with H141 and E277. The imidazole side chain of H141 is known to be hyper-reactive, and its chemical modification or mutagenesis is known to similarly compromise catalysis. The reactive substrate analogue 2(*S*)-amino-6-boronohexanoic acid (ABH) binds as a tetrahedral boronate anion to $Mn^{2+}_2$, $Co^{2+}_2$, $Ni^{2+}_2$, and $Zn^{2+}_2$ clusters in human arginase I, and it can be stabilized by a third inhibitory $Zn^{2+}$ ion coordinated by H141. Because ABH binds as an analogue of the tetrahedral intermediate and its flanking transition states in catalysis, this implies that the various metallo-substituted enzymes are capable of some level of catalysis with an actual substrate. Accordingly, we establish the following trend for turnover number ($k_{cat}$) and catalytic efficiency ($k_{cat}/K_M$): $Mn^{2+} > Ni^{2+} \approx Co^{2+} \gg Zn^{2+}$. Therefore, $Mn^{2+}$ is required for optimal catalysis by human arginase I.

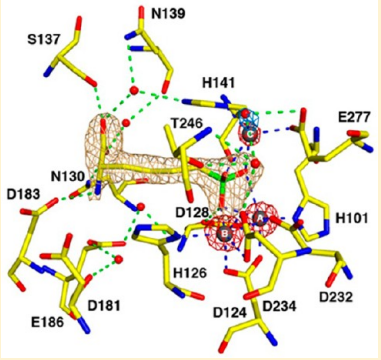


Human arginase I is a binuclear manganese metalloenzyme that catalyzes the hydrolysis of L-arginine (L-Arg) to form products L-ornithine (L-Orn) and urea during the final cytosolic step of the urea cycle.[1−3] As demonstrated for rat arginase I, a complete $Mn^{2+}_2$ cluster is required for maximal catalytic activity in vivo.[4,5] The same holds true for human arginase I; however, this enzyme can be reconstituted with a $Co^{2+}_2$ cluster that is said to yield 10-fold higher catalytic activity in vitro.[6] Early studies demonstrated that rat arginase I treated with metal ion chelators can be reconstituted with $Co^{2+}$, $Ni^{2+}$, and $Cd^{2+}$ to yield enzymes with 25−35% activity compared with that of $Mn^{2+}_2$-rat arginase I.[7] However, because chelators extract only one metal ion from the binuclear manganese cluster of rat arginase I,[8] the residual activity observed in early metal reconstitution experiments with this enzyme[7] most likely derived from mixed metal clusters. Significantly, metal binding properties and catalytic metal requirements can vary for arginases from different species. Indeed, certain bacterial arginases utilize binuclear metal clusters other than $Mn^{2+}_2$, such as the $Co^{2+}_2$ preference observed for the arginase from *Helicobacter pylori* or the $Ni^{2+}_2$ preference for the arginase from *Bacillus anthracis*.[9,10]

Metal coordination geometry in the active site of human arginase I is distorted octahedral for both metal ions in the native, unliganded enzyme,[11] and in the enzyme complex with the tetrahedral transition state analogue inhibitor 2(*S*)-amino-6-boronohexanoic acid (ABH),[12] which binds as the tetrahedral boronate anion (Figure 1).[13] Octahedral metal coordination polyhedra may account for the relative ease with which the $Mn^{2+}_2$ cluster is substituted with alternative metal ions that readily adopt octahedral metal coordination, such as $Co^{2+}$ and $Ni^{2+}$. Our recent crystal structure determinations of $Co^{2+}_2$-human arginase I and its complexes with ABH and the product L-Orn reveal identical metal coordination geometries compared to those observed in the corresponding complexes with $Mn^{2+}_2$-human arginase I.[14] If identical metal coordination geometries are presumed, activity differences among $Mn^{2+}_2$-, $Co^{2+}_2$-, and $Ni^{2+}_2$-substituted arginases may result in part from the differing abilities of each particular metal ion cluster in activating the catalytic nucleophile, believed to be a metal-bridging hydroxide ion,[1−3] and in stabilizing the tetrahedral intermediate and its flanking transition states in catalysis. For example, the 10-fold activity enhancement observed for L-Arg hydrolysis by $Co^{2+}_2$-human arginase I in comparison with $Mn^{2+}_2$-human arginase I is believed to result from a $pK_a$ for the $Co^{2+}$-bridging water molecule that is approximately 1 unit lower than that of the $Mn^{2+}$-bound water molecule, thereby resulting in a higher concentration of the nucleophilic metal-bridging hydroxide ion.[6]

It is currently unknown whether arginase reconstituted with a $Zn^{2+}_2$ cluster exhibits catalytic activity, despite the fact that $Zn^{2+}$ is ubiquitous in hydrolytic metalloenzymes, e.g., such as the prototypical metalloproteases carboxypeptidase A and thermolysin.[15,16] Although octahedral $Zn^{2+}$ coordination geometry in

**Received:** August 23, 2012
**Revised:** October 1, 2012
**Published:** October 12, 2012

  

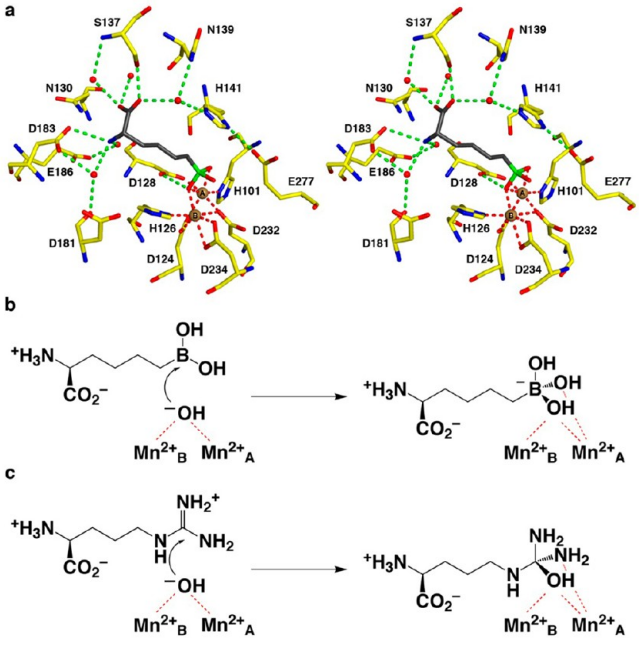


**Figure 1.** (a) Binding of the reactive substrate analogue inhibitor ABH in the active site of $Mn^{2+}{}_2$-human arginase I (PDB entry 2AEB), which mimics the binding of the tetrahedral intermediate and its flanking transition states in catalysis. Atoms are color-coded as follows: yellow for C, blue for N, red for O, green for B, brown spheres for $Mn^{2+}$, and red spheres for solvent. (b) The nucleophilic metal-bridging hydroxide ion of $Mn^{2+}{}_2$-human arginase I attacks the $sp^2$-hybridized boron atom in the trigonal planar boronic acid moiety of ABH to form a stable tetrahedral boronate anion. (c) The nucleophilic metal-bridging hydroxide ion of $Mn^{2+}{}_2$-human arginase I attacks the $sp^2$-hybridized carbon atom in the trigonal planar guanidinium group of substrate L-arginine to form a metastable tetrahedral intermediate during catalysis.

proteins is occasionally observed,[17,18] tetrahedral coordination geometry is more typically preferred because the $Zn^{2+}$ ion is not subject to ligand field stabilization energy.[19] Accordingly, the octahedral metal binding sites of arginase may not be ideal for $Zn^{2+}$ binding. Moreover, the binding of $Zn^{2+}$ to native arginase enzymes from various species is inhibitory.[20−23] This inhibition could result from association of $Zn^{2+}$ with an adventitious tetrahedral binding site formed by catalytic residues and metal-bound solvent molecules, as observed for the inhibition of carboxypeptidase A and thermolysin by excess $Zn^{2+}$.[24,25]

To understand the structural basis for activity differences in human arginase I containing $Mn^{2+}{}_2$, $Co^{2+}{}_2$, $Ni^{2+}{}_2$, and $Zn^{2+}{}_2$ clusters and to understand the structural basis for the inhibitory activity of $Zn^{2+}$ against $Mn^{2+}{}_2$-human arginase I, we now report X-ray crystal structures of human arginase I substituted with $Ni^{2+}$ or $Zn^{2+}$ in the presence and absence of the inhibitor ABH. Additionally, we show that the inhibitory effect of $Zn^{2+}$ against $Mn^{2+}{}_2$-human arginase I results from the formation of a novel trinuclear $Mn^{2+}{}_2Zn^{2+}$ cluster, in which the inhibitory $Zn^{2+}$ ion is liganded by active site residue H141 in alternate binding modes depending on whether ABH is also bound.

## EXPERIMENTAL PROCEDURES

**Materials.** Dipicolinic acid, manganese(II) chloride tetrahydrate (≥99%), cobalt chloride hexahydrate (>99%), and nickel chloride hexahydrate were purchased from Sigma. Tris(2-carboxyethyl)phosphine hydrochloride (TCEP, 98%) was purchased from Alfa Aesar. 2(*S*)-Amino-6-boronohexanoic acid (ABH) ammonium salt was purchased from Enzo Life Sciences (Farmingdale, NY). Prepared solutions of 50% (w/v) Jeffamine ED-2001 with 100 mM HEPES (pH 7.0) and 30% (v/v) Jeffamine ED-2001 with 100 mM HEPES (pH 7.0) were purchased from Hampton Research (Aliso Viejo, CA). Ethylenediaminetetraacetic acid tetrasodium salt (EDTA, 99.5%), zinc chloride (99.1%), and all other chemicals were purchased from Fisher Scientific.

**Expression and Purification of Metallo-Substituted Human Arginase I.** Human arginase I was expressed in *Escherichia coli* strain BL21-Gold (DE3) cells (Agilent Technologies) by transformation of the pBS(KS) plasmid.[13] A 2 mL starter culture containing Luria-Bertani medium and ampicillin at a final concentration of 100 μg/mL was grown for 8 h in a shaker at 37 °C and 250 rpm. A second starter culture (250 mL) containing a minimal medium recipe [minimal medium M9 salts (Sigma), casamino acids, 18 mM D-(+)-glucose (Acros, ACS reagent), 1.8 mM $MgSO_4$, 89 μM $CaCl_2$, and 100 μg/mL ampicillin] was inoculated with 500 μL of the 2 mL starter culture and incubated at 37 °C and 220 rpm for 14 h. Subsequently, 500 mL cultures in the minimal medium recipe were inoculated with 25 mL of the second starter culture and incubated at 37 °C and 220 rpm until the $OD_{600}$ reached 0.8−1.0. The incubating temperature was then lowered to 25 °C, and each culture was supplemented with 500 μL of 1 M IPTG and 500 μL of a 0.1 M solution of either $MnCl_2$, $CoCl_2$, $NiCl_2$, or $ZnCl_2$. Cultures were incubated at 25 °C and 220 rpm for 12 h. These cells were pelleted by centrifugation and stored at −80 °C.

Metal-substituted arginases were purified as described for the native enzyme[13] with slight modification. Briefly, the pelleted cells were thawed to room temperature and resuspended in a lysis buffer [10 mM Tris (pH 8.0), 150 mM NaCl, 1 mM EDTA, and either $MnCl_2$, $CoCl_2$, $NiCl_2$, or $ZnCl_2$ (5 mM)]. Cells were sonicated on ice using a Sonifier 450 (Branson) [33% duty cycle with maximum tip setting (#7)], and sonications were performed in three cycles (one cycle is sonication for 3 min followed by a 2 min rest period). The cell lysate was centrifuged at 15000 rpm for 45 min, after which the supernatant was recovered. In a round-bottom flask, the supernatant was heated and stirred gently at 50 °C for 20 min, then cooled on ice for 10 min, and finally centrifuged at 15000 rpm for 5 min. The supernatant was then heated again in a second round-bottom flask at 60 °C for 20 min, cooled on ice for 10 min, centrifuged at 15000 rpm for 15 min, and then dialyzed against 20 mM Tris (pH 7.5), 2 mM TCEP, and 1 mM EDTA; the preparation was subsequently equilibrated with either $MnCl_2$, $CoCl_2$, $NiCl_2$, or $ZnCl_2$ (2 mM). A carboxymethyl cellulose (CM-52) resin (Whatman) was sequentially washed with (1) 500 mL of deionized water, (2) 500 mL of a metal chelation buffer [100 mM Tris (pH 7.5), 150 mM NaCl, and 10 mM EDTA], and (3) 500 mL of deionized water over a sintered funnel (frit pore diameter of 10 − 20 μm) under vacuum. The washed resin, which was almost dry, was suspended in 80 mL of CM-52 mobile phase A [20 mM Tris (pH 7.5), 2 mM TCEP, 1 mM EDTA, and either $MnCl_2$, $CoCl_2$, $NiCl_2$, or $ZnCl_2$ (2 mM)]. A column was packed with CM-52 resin (3 cm inside diameter × 7 cm resin bed height) and equilibrated with mobile phase A. The dialysate was loaded onto the CM-52 column and was subjected to step elution with 100% mobilie phase B [20 mM Tris (pH 7.5), 2 mM TCEP, 300 mM NaCl, 1 mM EDTA, and either $MnCl_2$, $CoCl_2$, $NiCl_2$, or $ZnCl_2$ (2 mM)]. The eluted

enzyme was >98% pure as judged by sodium dodecyl sulfate–polyacrylamide gel electrophoresis analysis. Finally, the purified enzyme was exchanged into a final buffer of 50 mM bicine (pH 8.5) and either $MnCl_2$, $CoCl_2$, $NiCl_2$, or $ZnCl_2$ (100 $\mu$M) using a PD-10 desalting column (GE Healthcare).

**Activity Assays.** Arginase activity was monitored spectrophotometrically based on the formation of urea, using the colorimetric assay developed by Archibald.[26] All measurements were performed in quadruplicate at 22 °C. A stock solution of 100 mM L-Arg in 50 mM HEPPS (pH 8.5) and 100 $\mu$M $MCl_2$ (M = $Mn^{2+}$, $Co^{2+}$, or $Ni^{2+}$) was prepared. From this stock solution, 200 $\mu$L samples were prepared with a range of L-Arg concentrations (0.20–18.0 mM for $Mn^{2+}{}_2$-human arginase I, 0.06–9.1 mM for $Co^{2+}{}_2$-human arginase I, and 0.20–18.0 mM for $Ni^{2+}{}_2$-human arginase I) in 50 mM HEPPS (pH 8.5). Each reaction was initiated by the addition of 20 $\mu$L of 0.073 $\mu$M trimeric $Mn^{2+}{}_2$-human arginase I ($\varepsilon_{280}$ = 22990 $M^{-1}$ $cm^{-1}$ for the monomer) and terminated after 90 s (optimal time) using 30 $\mu$L of a 3:1 (v/v) concentrated acid/chromophore dye solution [$H_2SO_4$:$H_3PO_4$:$H_2O$ (1:3:1, v/v/v)/245 mM $\alpha$-isonitrosopropiophenone in ethanol]. Samples were heated to 90 °C for 1 h in a thermocycler to ensure complete reaction of urea with the dye. For the quantification of urea, 150 $\mu$L of each sample was transferred into a flat-bottom 96-well plate (Fisher) and spectrophotometric absorbance readings were recorded at 550 nm ($\lambda$) with an Envision plate reader (Perkin-Elmer) immediately after solutions had been heated. A urea standard curve was made every time the plate reader was used, and the concentrations of the urea standards ranged from 0 to 2.0 mM.

To confirm catalytic activity measurements for $Mn^{2+}{}_2$-human arginase I and $Co^{2+}{}_2$-human arginase I, arginase activity was also measured by a sensitive $^{14}C$ radioactive assay as described by Rüegg and Russell.[27] All measurements were performed in triplicate at 22 °C. Briefly, a typical reaction mixture contained 40 $\mu$L of assay buffer [50 mM HEPPS (pH 8.5), 0.02275 $\mu$M L-[*guanidino*-$^{14}C$]arginine, and either $MnCl_2$ or $CoCl_2$ (100 $\mu$M)] in each reaction tube. The L-[*guanidino*-$^{14}C$]arginine (specific activity of 55 mCi/mmol) was purchased from American Radiolabeled Chemicals. Typically, 5 $\mu$L of increasing concentrations of unlabeled L-Arg was added to each 40 $\mu$L reaction mixture such that final L-Arg concentrations ranged as follows: from 0.070 to 40 mM for $Mn^{2+}{}_2$-human arginase I and from 0.070 to 30 mM for $Co^{2+}{}_2$-human arginase I. Reactions were initiated by the addition of 5 $\mu$L of assay buffer containing the metal-reconstituted arginase (0.081 $\mu$M $Mn^{2+}{}_2$-human arginase I or 0.174 $\mu$M $Co^{2+}{}_2$-human arginase I). After 90 s, reactions were terminated by the addition of 200 $\mu$L of stop solution [0.25 M acetic acid (pH 4.5), 7 M urea, and 0.010 M unlabeled L-Arg], immediately followed by the addition of 200 $\mu$L of Dowex solution [1:1 (v/v) slurry of Dowex 50 W-X8 (Acros) in deionized water], and vortexed. Reaction samples were gently mixed for 10 min and centrifuged at 2000 rpm for 2 min. The supernatant from each reaction (200 $\mu$L) was added to 3.0 mL of Ecoscint solution (National Diagnostics) for liquid scintillation counting, which was performed using a Beckman model LS5000E counter.

**Inductively Coupled Plasma Mass Spectrometry (ICP-MS) Analysis.** Purified samples of $Mn^{2+}{}_2$-, $Co^{2+}{}_2$-, and $Ni^{2+}{}_2$-human arginase I were subjected to ICP-MS for the quantitative analysis of metal ion content and stoichiometry at the Center for Applied Isotope Studies, University of Georgia (Athens, GA). Each sample, which was initially solubilized in 50 mM bicine (pH 8.5) and either $MnCl_2$, $CoCl_2$, or $NiCl_2$ (100 $\mu$M), was subjected to a buffer exchange to minimize the free metal ion concentration in solution. A separate PD-10 column (GE Healthcare) was used for each sample. These columns were first washed with (1) 25 mL of deionized water or (2) 25 mL of a metal chelation solution [10 mM bicine (pH 8.5) and 5 mM EDTA] and then pre-equilibrated with 25 mL of 10 mM bicine (pH 8.5) prior to running each sample. Samples were dialyzed using dialysis cassettes (Pierce, 10 kDa molecular mass cutoff) against a total of 6 L of 10 mM bicine (pH 8.5) at 4 °C, with three buffer exchanges. All dialysis glassware was prewashed with the same metal chelation solution followed by rinsing with deionized water. Each sample was concentrated using an Amicon Ultra-4 (10 kDa molecular mass cutoff) centrifugal concentrator; the final volume was adjusted to 1.0 mL, and the protein concentration was determined by amino acid analysis at the W. M. Keck Biotechnology Resource Laboratory, Yale University School of Medicine (New Haven, CT).

**Preparation of Metallo-Substituted Crystalline Human Arginase I.** While the preparation of metal-substituted arginases for activity assays in solution is described above, we opted to prepare metal-substituted arginases in the crystal using the more rapid and efficient protocol that we previously developed for our X-ray crystallographic studies of $Co^{2+}{}_2$-human arginase I.[14] Briefly, human arginase I was expressed in *E. coli*, purified, and crystallized as previously described.[11,13] A 3 $\mu$L drop of enzyme solution [14.7 mg/mL $Mn^{2+}{}_2$-human arginase I ($\varepsilon_{280}$ = 22900 $M^{-1}$ $cm^{-1}$ for the monomer), 1.4 mM thymine, 50 mM bicine (pH 8.5), 100 $\mu$M $MnCl_2$] and a 3 $\mu$L drop of precipitant solution [30% (v/v) Jeffamine ED-2001 and 100 mM HEPES (pH 7.0)] were combined on a siliconized cover slide and equilibrated against 500 $\mu$L of a precipitant solution. Crystals of the unliganded enzyme grew within 5 days at room temperature. These crystals were soaked for 14 days in a buffer solution of 15 mM EDTA, 15 mM dipicolinic acid, 100 mM HEPES (pH 7.0), and 30% (v/v) Jeffamine ED-2001, and solutions were replenished daily. Both chelators (EDTA and dipicolinic acid) were required to ensure complete removal of $Mn^{2+}$ ions, as we previously demonstrated in the preparation of metal-free human arginase I.[14] Crystals of the metal-free enzyme were reconstituted with a $Ni^{2+}{}_2$ cluster at pH 7.0 by being soaked in a buffer solution containing 5 mM $NiCl_2$, 100 mM HEPES (pH 7.0), and 30% (v/v) Jeffamine ED-2001 for 26 h. A crystal of the $Ni^{2+}{}_2$-human arginase I complex with ABH was prepared by soaking a crystal of the metal-free enzyme in 5 mM $NiCl_2$, 5 mM ABH, 100 mM HEPES (pH 7.0), and 32% (w/v) Jeffamine ED-2001 for 26 h. A crystal of the $Zn^{2+}{}_5$-human arginase I–ABH complex was prepared by soaking a crystal of the metal-free enzyme in 5 mM $ZnCl_2$, 5 mM ABH, 100 mM HEPES (pH 7.0), and 30% (v/v) Jeffamine ED-2001 for 18 h. A crystal of the $Mn^{2+}{}_2Zn^{2+}$-human arginase I–ABH complex was prepared by soaking a crystal of $Mn^{2+}{}_2$-human arginase I in 5 mM $ZnCl_2$, 5 mM ABH, 100 mM HEPES (pH 7.0), and 32% (w/v) Jeffamine ED-2001 for 26 h. The unliganded $Mn^{2+}{}_2Zn^{2+}$-human arginase I complex was prepared by soaking a $Mn^{2+}{}_2$-human arginase I crystal in 5 mM $ZnCl_2$, 50 mM boric acid, 100 mM HEPES (pH 7.0), and 30% (v/v) Jeffamine ED-2001 for 26 h. All crystals were flash-cooled in liquid nitrogen with their respective mother liquor solutions serving as cryoprotectants.

**X-ray Crystal Structure Determinations.** X-ray diffraction data from single crystals of $Ni^{2+}{}_2$-human arginase I, the $Ni^{2+}{}_2$-human arginase I–ABH complex, the $Zn^{2+}{}_2$,$Zn^{2+}{}_{CD}$-

**Table 1. Data Collection and Refinement Statistics of Metallo-Substituted Human Arginase I**

| | $Ni^{2+}_2$ | $Ni^{2+}_2$, ABH complex | $Zn^{2+}_5$, ABH complex | $Mn^{2+}_2Zn^{2+}$ | $Mn^{2+}_2Zn^{2+}$, ABH complex |
|---|---|---|---|---|---|
| | | Data Collection | | | |
| resolution limits (Å) | 50.0−1.70 | 50.0−1.48 | 50.0−2.20 | 50.0−1.90 | 50.0−1.53 |
| total/unique reflections measured (no.) | 795439/70032 | 498285/106524 | 147051/32953 | 579461/51066 | 272261/97388 |
| space group symmetry | *P*3 | *P*3 | *P*3 | *P*3 | *P*3 |
| unit cell dimensions | | | | | |
| *a*, *b*, *c* (Å) | 90.35, 90.35, 69.81 | 90.71, 90.71, 69.66 | 91.12, 91.12, 69.77 | 90.83,90.83, 70.07 | 91.08, 91.08, 69.90 |
| *α*, *β*, *γ* (deg) | 90, 90, 120 | 90, 90, 120 | 90, 90, 120 | 90, 90, 120 | 90, 90, 120 |
| $R_{merge}$[a,b] | 0.093 (0.432) | 0.067 (0.354) | 0.096 (0.698) | 0.101 (0.978) | 0.069 (0.341) |
| $I/\sigma(I)$[a] | 26.53 (7.07) | 21.59 (4.36) | 14.20 (2.19) | 26.39 (2.67) | 15.50 (3.21) |
| completeness (%)[a] | 99.9 (100) | 99.8 (100) | 99.9 (100) | 99.9 (100) | 99.5 (98.2) |
| | | Refinement | | | |
| no. of reflections used in refinement/test set | 69431/3213 | 105002/5116 | 29796/1457 | 49137/2368 | 94853/4626 |
| twinning fraction | 0.50 | 0.45 | 0.21 | 0.50 | 0.47 |
| $R_{twin}$[c] | 0.1542 | 0.1531 | 0.1723 | 0.1540 | 0.1598 |
| $R_{twin/free}$[d] | 0.1889 | 0.1925 | 0.2328 | 0.2211 | 0.2153 |
| no. of solvent molecules[e] | 163 | 198 | 106 | 79 | 175 |
| no. of ligand molecules[e] | 0 | 2 | 2 | 0 | 2 |
| no. of metal ions[e] | 4 | 4 | 9 | 6 | 6 |
| root-mean-square deviation | | | | | |
| bonds (Å) | 0.008 | 0.007 | 0.008 | 0.008 | 0.008 |
| angles (deg) | 1.5 | 1.5 | 1.6 | 1.5 | 1.5 |
| average *B* factor (Å$^2$) | | | | | |
| main chain | 26 | 22 | 46 | 38 | 24 |
| side chain | 28 | 24 | 48 | 39 | 26 |
| solvent | 27 | 23 | 38 | 31 | 24 |
| ligand | − | 23 | 40 | − | 21 |
| metal ions[f] | 20 (4) | 17 (4) | 37 (9) | 30 (6) | 19 (6) |
| Ramachandran plot (%) | | | | | |
| allowed | 85.8 | 88.8 | 85.8 | 85.4 | 88.6 |
| additionally allowed | 13.8 | 10.8 | 13.4 | 13.8 | 11.0 |
| generously allowed | 0.2 | 0.0 | 0.6 | 0.6 | 0.0 |
| disallowed (Q65) | 0.2 | 0.4 | 0.2 | 0.2 | 0.4 |
| PDB entry | 4GSM | 4GSV | 4GSZ | 4GWC | 4GWD |

[a]Values in parentheses are for the highest-resolution shell. [b]$R_{merge} = \sum|I - \langle I\rangle|/\sum I$, where $I$ is the observed intensity and $\langle I\rangle$ is the average intensity calculated from replicate data. [c]$R_{twin} = \sum||F_o| - |F_c||/\sum|F_o|$ for reflections contained in the working set. [d]$R_{twin/free} = \sum||F_o| - |F_c||/\sum|F_o|$ for 5% of the reflections contained in the test set held aside during refinement. $|F_o|$ and $|F_c|$ are the observed and calculated structure factor amplitudes, respectively. [e]Per asymmetric unit cell. [f]Values in parentheses indicate the total number of metal ions in the unit cell for each structure from which the average *B* factor was calculated.

human arginase I−ABH complex, and the $Mn^{2+}_2,Zn^{2+}_{CD}$-human arginase I−ABH complex, the inhibitor-free $Mn^{2+}_2,Zn^{2+}_{CE}$-human arginase I complex were collected on beamline X29 ($\lambda$ = 1.075 Å) of the National Synchrotron Light Source at Brookhaven National Laboratory (Upton, NY). Diffraction data were indexed, integrated, and scaled using the *HKL-2000* suite of programs.[28] All crystals were hemihedrally twinned, as initially reported for the $Mn^{2+}_2$-human arginase I−ABH complex,[13] and belonged to apparent space group *P*3 with similar unit cell dimensions (Table 1). Structures were determined by molecular replacement using *Phaser* as implemented in the *CCP4* suite of programs.[29,30] The search model used for rotation and translation function calculations was the A-chain structure of $Mn^{2+}_2$-human arginase I (PDB entry 2PHA[11]) less metal ions and solvent atoms (for structures with intact binuclear manganese clusters, only solvent atoms were omitted).

Refinement was performed with CNS (version 1.2)[31] using the hemihedral twinning operation parameters −*h*, −*k*, and *l*; the twinning fraction varied slightly from one structure to another (Table 1). Model building was performed using *Coot* (version 0.6.1).[32] Atomic coordinates of the bound inhibitor ABH and water molecules were included in the later stages of refinement. For the $Ni^{2+}_2$-human arginase I−ABH, $Zn^{2+}_5$-human arginase I−ABH, and $Mn^{2+}_2Zn^{2+}$-human arginase I−ABH complexes, gradient omit maps showed ABH bound in the active site of each monomer in the asymmetric unit, and all ABH atoms were refined with full occupancy. In addition, average *B* factors for ABH in these complexes were similar to the main chain average *B* factors for the entire protein (Table 1).

In all the crystal structures reported herein, metal ion sites A and B were refined with full occupancy. For the $Zn^{2+}_5$-human arginase I−ABH complex, metal ion sites CD, D, and E were refined with occupancy values of 0.55, 0.35, and 0.35, respectively (reported occupancy values are averaged over all monomers in the asymmetric unit). For the $Mn^{2+}_2Zn^{2+}$-human arginase I structure, metal ion site CE was refined with an occupancy of 0.48. For the $Mn^{2+}_2Zn^{2+}$-human arginase I−ABH complex, metal ion site CD was refined to full occupancy. The average *B* factors for metal ions were slightly lower than the average *B* factors for main chain atoms in each structure.

Disordered segments at the N-terminus (residues M1−S5) and at the C-terminus (residues P320−K322) were excluded from all final models. For unliganded $Ni^{2+}_2$-human arginase I, unliganded $Mn^{2+}_2Zn^{2+}$-human arginase I, and the $Zn^{2+}_5$-human arginase I−ABH complex, Q65 in monomer A of the asymmetric unit adopts a disallowed conformation based on the Ramachandran plot (data not shown). For the $Ni^{2+}_2$-human arginase I−ABH complex and the $Mn^{2+}_2Zn^{2+}$-human arginase I−ABH complex, Q65 adopts a disallowed conformation in both monomers A and B of the asymmetric unit. Because the main chain atoms of Q65 are characterized by clear and unambiguous electron density, this is not likely to be an artifact. Ramachandran statistics were calculated with PROCHECK,[33] and average *B* factors were calculated with MOLEMAN.[34] Data collection and refinement statistics for all structure determinations are listed in Table 1.

## RESULTS

**Catalytic Activity Measurements.** Using the colorimetric assay developed by Beale and Croft,[35] Stone and colleagues[6] report that $Co^{2+}_2$-human arginase I at 37 °C exhibits a $k_{cat}$ of 240 ± 14 $s^{-1}$, a $K_M$ of 0.19 ± 0.04 mM, and a $k_{cat}/K_M$ of 1270 ± 330 $mM^{-1}$ $s^{-1}$ at pH 7.4; notably, the catalytic efficiency ($k_{cat}/K_M$) is said to be 10-fold higher than that measured for $Mn^{2+}_2$-human arginase I ($k_{cat}$ = 300 ± 12 $s^{-1}$, $K_M$ = 2.33 ± 0.26 mM, and $k_{cat}/K_M$ = 129 ± 20 $mM^{-1}$ $s^{-1}$ at pH 7.4). However, we obtain slightly different results using the colorimetric assay developed by Archibald[26] and the radioactive L-[*guanidino*-$^{14}$C]-arginine assay of Rüegg and Russell[27] (Table 2). A possible reason for these differences is the two different oxime reagents used for urea quantification in the colorimetric assays. The assay pH may also contribute to the observed activity differences; Stone and colleagues[6] report measurements at pH 7.4, whereas our measurements were taken at pH 8.5, close to the pH optimum for catalytic activity. We were not able to prepare $Zn^{2+}_2$-human arginase I because of protein precipitation. For each soluble metallo-substituted arginase, ICP-MS measurements confirm the incorporation of the desired metal ions without contamination by other adventitious metal ions (Table 3). The trend in turnover number ($k_{cat}$) and catalytic efficiency ($k_{cat}/K_M$) for metallo-substituted human arginase I is as follows: $Mn^{2+}$ > $Ni^{2+}$ ≈ $Co^{2+}$ ≫ $Zn^{2+}$ ($Zn^{2+}$ is always inhibitory).

Table 2. Catalytic Activities of Metallo-Substituted Enzymes

| enzyme | $K_M$ (mM) | $k_{cat}$ ($s^{-1}$) | $k_{cat}/K_M$ ($\times 10^4$ $M^{-1}$ $s^{-1}$) |
|---|---|---|---|
| $Mn^{2+}_2$-human arginase I[a] | 3 ± 1 | 340 ± 160 | 11 ± 2 |
| $Co^{2+}_2$-human arginase I[a] | 1.7 ± 0.3 | 90 ± 60 | 6 ± 4 |
| $Ni^{2+}_2$-human arginase I[a] | 4 ± 1 | 110 ± 70 | 3 ± 1 |
| $Mn^{2+}_2$-human arginase I[b] | 8 ± 3 | 410 ± 120 | 5.4 ± 0.6 |
| $Co^{2+}_2$-human arginase I[b] | 3.7 ± 0.3 | 100 ± 10 | 2.6 ± 0.3 |

[a]Colorimetric assay, measurements in quadruplicate. [b]Radioactive L-[*guanidino*-$^{14}$C]arginine assay, measurements in triplicate.

**$Ni^{2+}_2$-Human Arginase I.** The overall structure of unliganded $Ni^{2+}_2$-human arginase I is essentially identical to that of $Mn^{2+}_2$-human arginase I (PDB entry 2PHA[11]), with a root-mean-square deviation (rmsd) of 0.24 Å for 313 C$\alpha$ atoms. The coordination numbers and geometries of $Ni^{2+}_A$ and $Ni^{2+}_B$ are essentially identical to those observed for the corresponding metal ions in unliganded $Mn^{2+}_2$-human arginase I and $Co^{2+}_2$-human arginase I.[11,14] However, the average metal−metal separation in $Ni^{2+}_2$-human arginase I is 3.2 Å, which is slightly shorter than that observed in $Mn^{2+}_2$- and $Co^{2+}_2$-human arginase I (3.4 Å each). Furthermore, the average metal coordination distances are generally shorter in $Ni^{2+}_2$-human arginase I: the average $Ni^{2+}$−ligand separation is 2.2 Å in $Ni^{2+}_2$-human arginase I at pH 7.0, whereas the average $Mn^{2+}$−ligand separation is 2.4 Å in $Mn^{2+}_2$-human arginase I at pH 7.5 (PDB entry 2PHA[11]). For comparison, the average $Co^{2+}$−ligand separation in $Co^{2+}_2$-human arginase I is 2.2 Å at pH 7.0 and 8.5 (PDB entries 3TH7 and 3THE, respectively).[14] It is interesting to note that the trend in average metal−ligand separations is consistent with the Irving−Williams series, which suggests generally weaker metal−ligand coordination interactions for $Mn^{2+}$ compared with those of $Co^{2+}$ or $Ni^{2+}$.

**$Ni^{2+}_2$-Human Arginase I−ABH Complex.** The overall fold of the $Ni^{2+}_2$-human arginase I−ABH complex is essentially identical to that of the $Mn^{2+}_2$-human arginase I−ABH complex (PDB entry 2AEB[13]), with an rmsd of 0.21 Å for 313 C$\alpha$ atoms. The average metal−metal separation in $Ni^{2+}_2$-human arginase I is 3.2 Å, which is close to that measured in the $Mn^{2+}_2$-human arginase I−ABH complex (3.3 Å) and equal to that measured in the $Co^{2+}_2$-human arginase I−ABH complex (3.2 Å) (PDB entries 2AEB and 3THH, respectively).[13,14] Interestingly, binding of ABH to $Ni^{2+}_2$-human arginase I does not change the average metal−metal separation, but binding of ABH to $Mn^{2+}_2$- and $Co^{2+}_2$-human arginase I slightly decreases the average metal−metal separation.

Upon binding to the enzyme, the boronic acid moiety of ABH undergoes nucleophilic attack by the metal-bridging hydroxide ion of the native $Ni^{2+}_2$-substituted enzyme to yield a tetrahedral boronate anion that mimics the tetrahedral intermediate and its flanking transition states in catalysis. The fact that the metal-bridging hydroxide ion in $Ni^{2+}_2$-human arginase I is sufficiently nucleophilic to react with ABH suggests that it is sufficiently nucleophilic to react with the actual substrate L-arginine, thereby accounting for the significant catalytic activity measured for $Ni^{2+}_2$-human arginase I (Table

Table 3. ICP-MS Analysis

| | metal:protein molar ratio[a] | | | | | |
|---|---|---|---|---|---|---|
| enzyme | Fe | Mn | Co | Ni | Cu | Zn |
| $Mn^{2+}_2$-human arginase I | 0.01 | 1.76 | 0.00 | 0.00 | 0.00 | 0.02 |
| $Co^{2+}_2$-human arginase I | 0.08 | 0.04 | 1.82 | 0.00 | 0.00 | 0.03 |
| $Ni^{2+}_2$-human arginase I | 0.02 | 0.03 | 0.00 | 1.47 | 0.00 | 0.04 |

[a]The metal ion content of metallo-substituted human arginase I was determined by ICP-MS, and the protein concentration was determined by amino acid analysis. The metal:protein ratio was determined by dividing the metal content (determined by ICP-MS) by the protein concentration (i.e., the concentration of arginase monomer).


dx.doi.org/10.1021/bi301145n | *Biochemistry* 2012, 51, 8399−8409

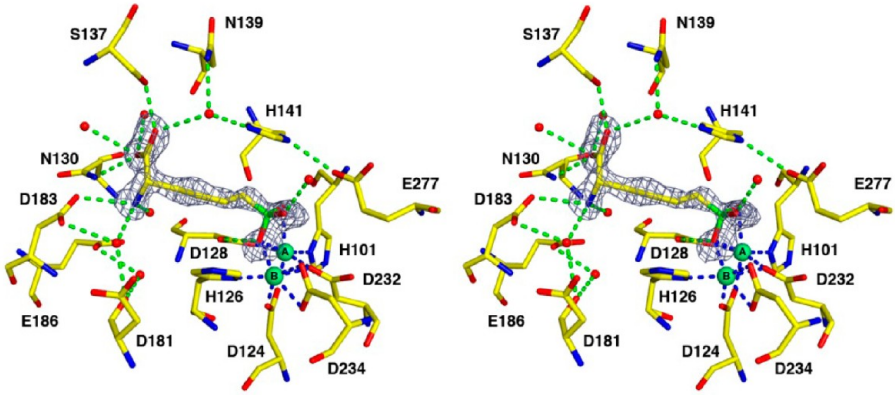


**Figure 2.** Omit map of the inhibitor ABH bound in the active site of $Ni^{2+}_2$-human arginase I, contoured at 3.4$\sigma$. Atoms are color-coded as follows: yellow for C, blue for N, red for O, green for B, light green spheres for $Ni^{2+}$, and red spheres for solvent. Metal coordination and hydrogen bond interactions are represented by blue and green dashed lines, respectively.

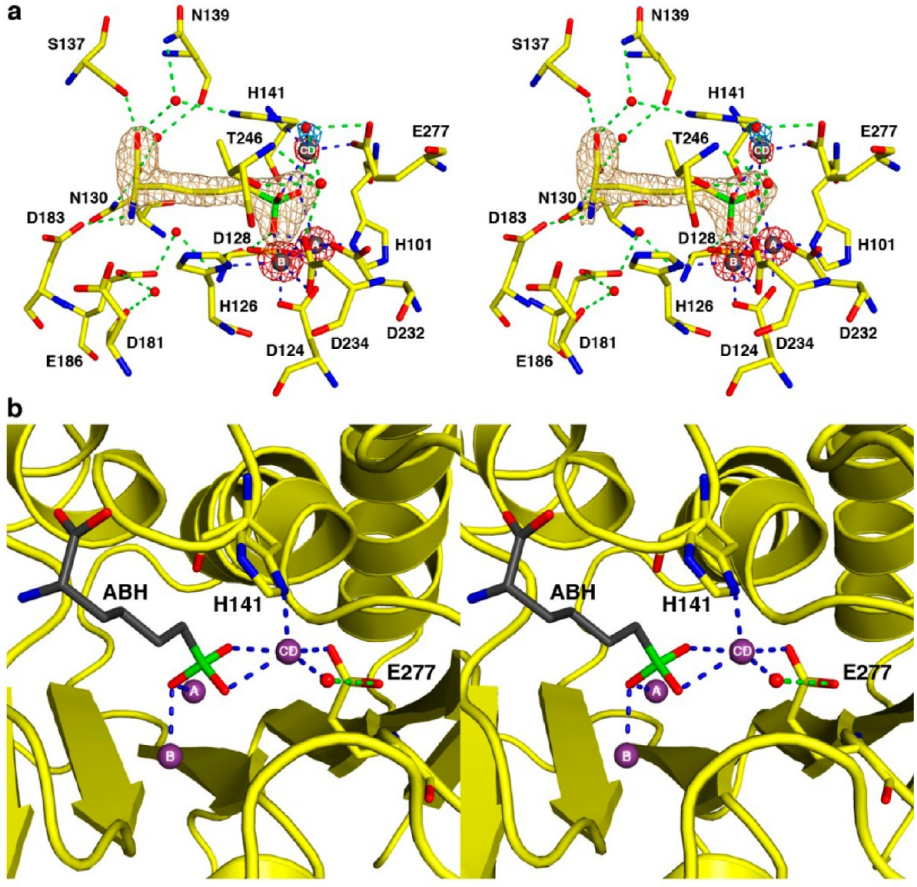


**Figure 3.** (a) Simulated annealing omit maps of the inhibitor ABH (tan, contoured at 5.5$\sigma$), three $Zn^{2+}$ ions (red, contoured at 14$\sigma$), and the $Zn^{2+}_{CD}$-bound water molecule (blue, contoured at 6.5$\sigma$) in the active site of the $Zn^{2+}_{S}$-human arginase I–ABH complex. Atoms are color-coded as follows: yellow for C, blue for N, red for O, green for B, dark gray spheres for $Zn^{2+}$, and red spheres for solvent. Metal coordination and hydrogen bond interactions are represented by blue and green dashed lines, respectively. (b) Another orientation of the complex shown in panel a highlights the square pyramidal coordination geometry of the $Zn^{2+}_{CD}$ ion.

2).[6] An omit map showing the bound inhibitor is found in Figure 2.

In the enzyme–inhibitor complex, boronate atom O1 coordinates to the $Ni^{2+}_A$ and $Ni^{2+}_B$ ions with an average separation of 2.3 Å; this atom corresponds to the metal-bridging hydroxide ion observed in the unliganded enzyme. Boronate atom O2 coordinates to $Ni^{2+}_A$ with an average interatomic separation of 2.4 Å. Boronate atom O3 hydrogen bonds with a water molecule that in turn is hydrogen bonded with the side chain of T246. Interestingly, the average metal–ligand separations are nearly equal in the $Ni^{2+}_2$-, $Co^{2+}_2$-, and $Mn^{2+}_2$-human arginase I–ABH complexes (2.3, 2.2, and 2.2 Å, respectively), in contrast with the trend observed for the unliganded metal-substituted enzymes. Finally, the $\alpha$-carbox-


dx.doi.org/10.1021/bi301145n | *Biochemistry* 2012, 51, 8399–8409

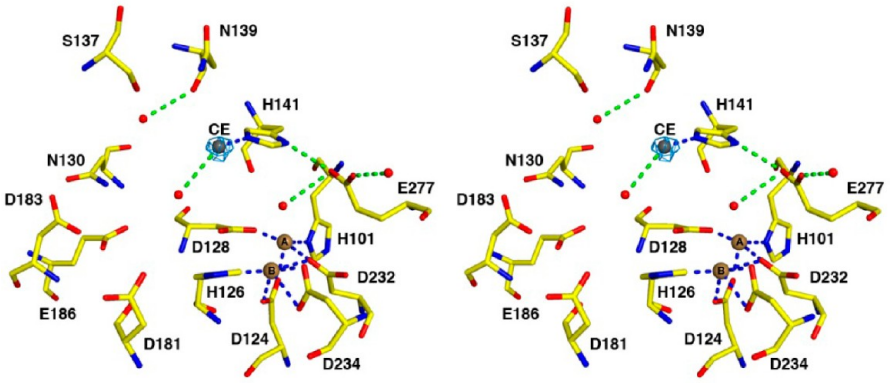


**Figure 4.** Simulated annealing omit map (blue) of the $Zn^{2+}_{CE}$ ion in the active site of monomer B of $Mn^{2+}_2Zn^{2+}$-human arginase I (contoured at 5.2$\sigma$), where it is coordinated by the N$\varepsilon$ atom of the H141 imidazole group. Formation of the carboxylate−histidine−zinc interaction with E277 and H141 is the structural basis for inhibition of arginase by zinc. Atoms are color-coded as follows: yellow for C, blue for N, red for O, brown spheres for $Mn^{2+}$, dark gray sphere for $Zn^{2+}$, and red spheres for solvent. Metal coordination and hydrogen bond interactions are represented by blue and green dashed lines, respectively. The solvent molecule near the $Mn^{2+}$ ions is too distant to be considered an inner-sphere ligand ($Mn^{2+}_A$−O and $Mn^{2+}_B$−O separations of 2.9 and 3.4 Å, respectively).

ylate and $\alpha$-amino groups of ABH make the same array of hydrogen bond interactions observed in the $Mn^{2+}_2$- and $Co^{2+}_2$-human arginase I−ABH complexes.[13,14]

**$Zn^{2+}_5$-Human Arginase I−ABH Complex.** When crystalline metal-free human arginase I is reconstituted with $Zn^{2+}$ and ABH, a total of five $Zn^{2+}$ ions are observed to bind, three of which are located in the active site. The overall structure of the $Zn^{2+}_5$-human arginase I−ABH complex at pH 7.0 is very similar to that of the $Mn^{2+}_2$-human arginase I−ABH complex (PDB entry 2AEB[13]), with an rmsd of 0.29 Å for 313 C$\alpha$ atoms. In the active site, metal ion binding sites A and B have been successfully reconstituted with $Zn^{2+}$ ions, and ABH binds as the tetrahedral boronate anion in a fashion identical to that observed in the $Mn^{2+}_2$-, $Co^{2+}_2$-, and $Ni^{2+}_2$-human arginase I−ABH complexes.[13,14] Strikingly, a third $Zn^{2+}$ ion binds in the active site and is coordinated by the N$\delta$ atom of the H141 imidazole group, the O$\varepsilon$1 atom of E277, boronate hydroxyl groups O2 and O3 of ABH, and a water molecule; the zinc-bound water molecule donates a hydrogen bond to the O$\varepsilon$2 atom of E277. However, the geometry of the latter interaction is poor, so it is likely to be a weak hydrogen bond at best. This new metal binding site is designated as site CD. Average metal−metal separations in the trinuclear zinc cluster are as follows: $Zn^{2+}_A$−$Zn^{2+}_B$, 3.4 Å; $Zn^{2+}_B$−$Zn^{2+}_{CD}$, 5.2 Å; $Zn^{2+}_A$−$Zn^{2+}_{CD}$, 4.7 Å. A simulated annealing omit map showing the bound inhibitor and active site $Zn^{2+}$ ions is shown in Figure 3a.

The fact that ABH binds to $Zn^{2+}$-substituted human arginase I as a tetrahedral boronate anion indicates that a possible metal-bridging hydroxide ion in native $Zn^{2+}_2$-human arginase I is sufficiently nucleophilic to attack the electrophilic boronic acid moiety of ABH, suggesting that nucleophilic attack at the guanidinium group of the actual substrate, L-arginine, could be possible. However, the binding of the $Zn^{2+}_{CD}$ ion further stabilizes the tetrahedral boronate anion, so it is possible that the binding of this tetrahedral species is mainly observed due to the additional metal coordination interactions with $Zn^{2+}_{CD}$, assuming that free $Zn^{2+}$ in solution does not affect the equilibrium between the boronic acid and boronate anion forms of ABH. We were unable to prepare protein or protein crystals containing solely a $Zn^{2+}_2$ cluster in the active site, so we are unable to draw any conclusions regarding the possible catalytic activity of $Zn^{2+}_2$-human arginase I. Presumably, however, catalytic activity would be minimal because of the facile inhibition by excess $Zn^{2+}$.

The $Zn^{2+}_{CD}$ ion has a coordination number of 5 and adopts an approximately square pyramidal coordination geometry (Figure 3b), with four oxygen atoms in equatorial positions and a nitrogen atom in the axial position. Notably, while coordination of $Zn^{2+}_{CD}$ by E277 is characterized by an average separation of 2.2 Å, indicative of a strong electrostatic interaction, the $Zn^{2+}_{CD}$ ion is located perpendicular to the plane of the E277 carboxylate, which constitutes poor geometry for a carboxylate−metal ion coordination interaction.[36]

Parenthetically, we note that two additional $Zn^{2+}$ ions are observed in this structure. First, the side chain of H312 near the C-terminus coordinates to a $Zn^{2+}$ ion at the contact surface between two monomers, approximately 15 Å from the active site (data not shown). Metal ion binding causes some minor conformational changes in the polypeptide segment flanking H312. This $Zn^{2+}$ ion, designated $Zn^{2+}_D$, is refined with an occupancy of 0.35. Finally, an additional metal ion, designated $Zn^{2+}_E$, is found on the protein surface coordinated by side chains of H115 and D117 and a water molecule. The $Zn^{2+}_E$ ion is refined with an occupancy of 0.35 in chains A and B (data not shown).

**$Mn^{2+}_2Zn^{2+}$-Human Arginase I.** The overall structure of unliganded $Mn^{2+}_2Zn^{2+}$-human arginase I is very similar to that of unliganded $Mn^{2+}_2$-human arginase I (PDB entry 2PHA[11]), with an rmsd of 0.31 Å for 313 C$\alpha$ atoms. Metal coordination interactions in the binuclear manganese cluster are similar to those observed in native unliganded $Mn^{2+}_2$-human arginase I, and the average $Mn^{2+}_A$−$Mn^{2+}_B$ separation is 3.2 Å. However, a $Zn^{2+}$ ion is coordinated by the N$\varepsilon$ atom and not the N$\delta$ atom of the H141 imidazole group (Figure 4), so the position of this $Zn^{2+}$ ion differs from that of the $Zn^{2+}_{CD}$ ion described above. Accordingly, we designate this new position as metal binding site CE. The H141 N$\delta$-H group donates a hydrogen bond to E277 with an average N−O separation of 2.9 Å. This interaction appears to be stronger than that in the $Zn^{2+}$-free enzyme, in which the corresponding average separation is 3.5 Å. It is likely that metal coordination by the N$\varepsilon$ atom of H141 increases the partial positive charge on the H141 N$\delta$-H group, thereby enhancing the favorable electrostatic interaction with E277.


dx.doi.org/10.1021/bi301145n | *Biochemistry* 2012, 51, 8399−8409

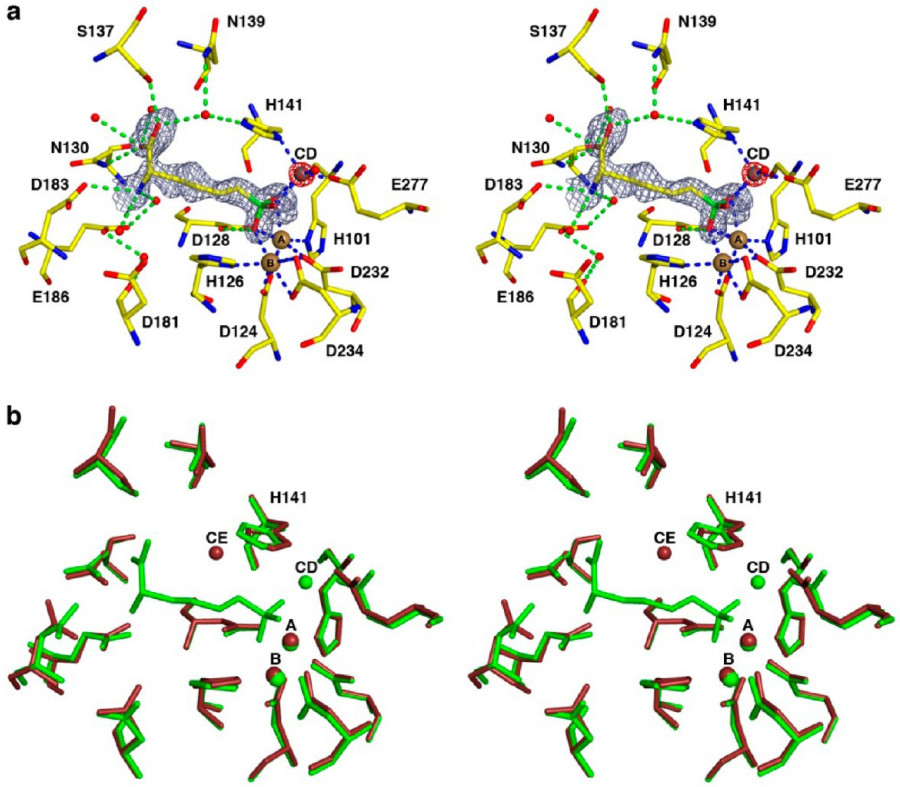


**Figure 5.** (a) Simulated annealing omit map of the inhibitor ABH (gray, contoured at 2.2$\sigma$) and the $Zn^{2+}{}_{CD}$ ion (red, contoured at 12$\sigma$) bound in the active site of the $Mn^{2+}{}_2Zn^{2+}$-human arginase I–ABH complex. Atoms are color-coded as follows: yellow for C, blue for N, red for O, brown spheres for $Mn^{2+}$, dark gray sphere for $Zn^{2+}$, and red spheres for solvent. Metal coordination and hydrogen bond interactions are represented by blue and green dashed lines, respectively. (b) Superposition of the $Mn^{2+}{}_2Zn^{2+}$-human arginase I–ABH complex (chain A, all atoms green) and $Mn^{2+}{}_2Zn^{2+}$-human arginase I (chain A, all atoms brown) highlights the different modes of binding of the inhibitory zinc ion to H141 in the unliganded and liganded forms of the enzyme.

The $Zn^{2+}{}_{CE}$ ion has only two ordered ligands, H141 and a water molecule; in chain A, this water molecule receives a hydrogen bond from R21. Parenthetically, we note that this complex does not contain a $Zn^{2+}{}_D$ or $Zn^{2+}{}_E$ ion bound to the surface sites observed in the $Zn^{2+}{}_5$-human arginase I–ABH complex. This crystal structure shows that the inhibition[20−23] of arginase by $Zn^{2+}$ results from the coordination of H141 to $Zn^{2+}$. This is consistent with mutagenesis studies of H141 in rat liver arginase demonstrating the catalytic importance of this residue.[37,38]

**$Mn^{2+}{}_2Zn^{2+}$-Human Arginase I–ABH Complex.** The structure of the $Mn^{2+}{}_2Zn^{2+}$-human arginase I–ABH complex is essentially identical to that of the $Mn^{2+}{}_2$-human arginase I–ABH complex (PDB entry 2AEB[13]), with an rmsd of 0.26 Å for 313 C$\alpha$ atoms. This complex contains the $Zn^{2+}{}_{CD}$ ion coordinated by the N$\delta$ atom of H141, the O$\varepsilon$1 atom of E277, boronate hydrogen groups O1 and O2 of ABH, and a water molecule (Figure 5a). This structure lacks the $Zn^{2+}{}_D$ and $Zn^{2+}{}_E$ ions as observed in the $Zn^{2+}{}_5$-human arginase I–ABH complex. Average metal–metal separations in the trinuclear metal cluster are as follows: $Mn^{2+}{}_A$–$Mn^{2+}{}_B$, 3.3 Å; $Mn^{2+}{}_B$–$Zn^{2+}{}_{CD}$, 4.9 Å; $Mn^{2+}{}_A$–$Zn^{2+}{}_{CD}$, 4.5 Å. Notably, the binding of $Zn^{2+}{}_{CD}$ does not perturb the average $Mn^{2+}{}_A$–$Mn^{2+}{}_B$ separation, which is also 3.3 Å in the $Mn^{2+}{}_2$-human arginase I–ABH complex. Metal ions $Mn^{2+}{}_A$, $Mn^{2+}{}_B$, and $Zn^{2+}{}_{CD}$ are coordinated with geometries identical to those observed for $Zn^{2+}{}_A$, $Zn^{2+}{}_B$, and $Zn^{2+}{}_{CD}$ in the structure of the $Zn^{2+}{}_5$-human arginase I–ABH complex. A superposition of the structure of the $Mn^{2+}{}_2Zn^{2+}$-human arginase I–ABH complex with that of unliganded $Mn^{2+}{}_2Zn^{2+}$-human arginase I shows the change in coordination of H141 to the inhibitory $Zn^{2+}$ ion, i.e., the $Zn^{2+}{}_{CE}$ → $Zn^{2+}{}_{CD}$ transition, triggered by the binding of ABH (Figure 5b).

## DISCUSSION

The X-ray crystal structure of unliganded $Mn^{2+}{}_2Zn^{2+}$-human arginase I is the first to reveal the structural basis for inhibition by $Zn^{2+}$. In this structure, a carboxylate–histidine–metal triad that involves E277, H141, and $Zn^{2+}{}_{CE}$ is fully formed. In such a triad, the basicity of the histidine imidazole for metal ion coordination is enhanced by the carboxylate group, and the acidity of the histidine imidazole for hydrogen bonding to the carboxylate is enhanced.[39] In $Mn^{2+}{}_2Zn^{2+}$-human arginase I, the binding of $Zn^{2+}{}_{CE}$ significantly strengthens the hydrogen bond interaction between E277 and H141, as reflected by the shorter E277–H141 separation of 2.8 Å in the fully formed triad compared with the separation of 3.5 Å in the native, unliganded enzyme.[11] Formation of the triad renders H141 nonfunctional in catalysis, where it is believed to act as a proton shuttle. In accord with these results, mutation or chemical modification of H141 results in significant but usually not complete loss of catalytic activity in rat arginase I[37,38,40] and in human arginase I.[41,42] For example, H141N and H141A rat arginases I exhibit 11 and 0.2% residual catalytic activity, respectively, compared to that of the wild-type enzyme based on $k_{cat}$.[37,38] These activity losses are consistent with the loss of an active site general base/general acid for which less efficient rescue pathways might be


dx.doi.org/10.1021/bi301145n | Biochemistry 2012, 51, 8399–8409

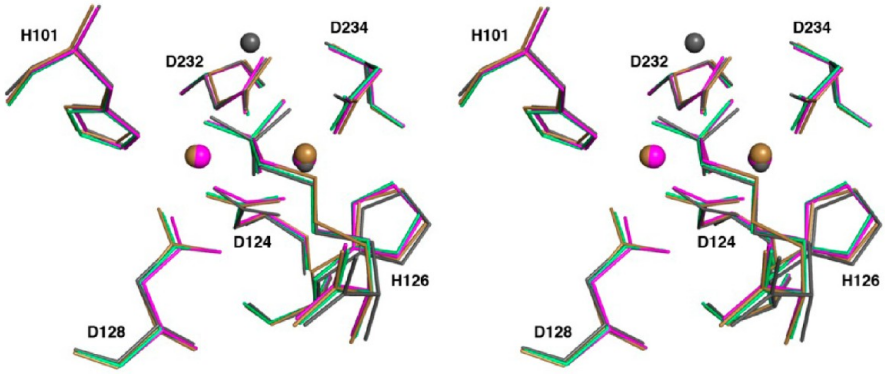


**Figure 6.** (a) Superposition of the A chains of the $Mn^{2+}_2$-human arginase I–ABH complex (PDB entry 2AEB, brown), the $Co^{2+}_2$-human arginase I–ABH complex (PDB entry 3THH, magenta), the $Ni^{2+}_2$-human arginase I–ABH complex (light green), and the $Zn^{2+}_5$-human arginase I–ABH complex (gray).

available, e.g., involving buffer and/or solvent molecules. Accordingly, compromising the function of a general base/general acid histidine imidazole group by coordination of an inhibitory $Zn^{2+}$ ion is particularly effective.

Metal ion sites A and B have distorted octahedral geometry in $Mn^{2+}_2$-human arginase I, and it is notable that this geometry is preserved regardless of what metal ions are substituted into or added to the enzyme active site (Figure 6). Curiously, however, we were unable to prepare crystals of unliganded $Zn^{2+}_2$-human arginase I. Our attempts to prepare crystals of this particular unliganded metalloenzyme resulted in substantial physical deterioration of the crystals during soaking experiments in buffer solutions containing 5 mM $ZnCl_2$, making the crystals unsuitable for X-ray diffraction experiments. Even so, we were able to reconstitute the enzyme with a $Zn^{2+}_3$ cluster in the active site, but only in the presence of the inhibitor ABH. Possibly, the binding of $Zn^{2+}$ ions to the distorted octahedral ligand fields in sites A and B is sufficiently stabilized only when ABH is bound, such that additional stabilization is derived from ABH coordination interactions with $Zn^{2+}_{CD}$.

Even so, it is conceivable that $Zn^{2+}_2$-human arginase I could catalyze the hydrolysis of L-Arg to form products L-Orn and urea because the crystal structure of the $Zn^{2+}_5$-human arginase I–ABH complex reveals that ABH also binds as the tetrahedral boronate anion (Figure 3a). As mentioned previously, the binding of ABH as a boronate anion requires a chemically reactive metal-bridging hydroxide ion that would be similarly reactive against the L-Arg substrate. However, because the third $Zn^{2+}$ ion binds readily in the active site as $Zn^{2+}_{CD}$ or $Zn^{2+}_{CE}$, catalytic turnover with the L-Arg substrate is prevented.

Finally, it is notable that human arginase I is capable of dissociation of the metal ion from sites A and B when the crystalline enzyme is dialyzed for 1 week against the metal ion chelators EDTA and dipicolinic acid at pH 7.0.[14] This feature allows structure–function studies of multiple metal-substituted arginases for the first time ever. While rat arginase I was the first arginase to yield a crystal structure,[43] complete metal ion extraction could not be achieved with this enzyme: only the $Mn^{2+}_A$ ion could be removed[8] and the protein precipitated if more aggressive dialysis conditions were utilized. Nevertheless, reconstitution of metal-depleted $Mn^{2+}_B$-rat arginase I with different metal ions resulted in the formation of hetereonuclear metal clusters,[5] some of which appeared to be functional. For example, $Mn^{2+}Co^{2+}$ and $Mn^{2+}Cd^{2+}$ clusters in H101N rat arginase I restore some, but not all, of the catalytic function of $Mn^{2+}_2$-H101N rat arginase I, which itself exhibits ~50% activity compared with that of the wild-type enzyme.[8,37] We conclude that rat and human arginase I are versatile systems for the preparation and study of homonuclear and heteronuclear metal clusters in a metalloprotein, and these systems will prove to be quite useful as we continue to probe the metal-dependent catalytic versatility of these enzymes.

## ■ ASSOCIATED CONTENT

### Accession Codes

The atomic coordinates and structure factors of $Ni^{2+}_2$-human arginase I, the $Ni^{2+}_2$-human arginase I–ABH complex, the $Zn^{2+}_5$-human arginase I–ABH complex, $Mn^{2+}_2Zn^{2+}$-human arginase I, and the $Mn^{2+}_2Zn^{2+}$-human arginase I–ABH complex have been deposited in the Protein Data Bank as entries 4GSM, 4GSV, 4GSZ, 4GWC, and 4GWD, respectively.

## ■ AUTHOR INFORMATION

### Corresponding Author

*Telephone: (215) 898-5714. Fax: (215) 573-2201. E-mail: chris@sas.upenn.edu.

### Funding

This work was supported by National Institutes of Health Grant GM49758.

### Notes

The authors declare no competing financial interest.

## ■ ACKNOWLEDGMENTS

We thank the National Synchrotron Light Source at Brookhaven National Laboratory (beamline X29) for access to X-ray crystallographic data collection facilities. Additionally, we thank Dr. Mustafa Köksal for helpful discussions.

## ■ ABBREVIATIONS

L-Arg, L-arginine; L-Orn, L-ornithine; ABH, 2(*S*)-amino-6-boronohexanoic acid; EDTA, ethylenediaminetetraacetic acid; HEPES, *N*-(2-hydroxyethyl)piperazine-*N*′-(2-ethanesulfonic acid); HEPPS, *N*-(2-hydroxyethyl)piperazine-*N*′-(3-propanesulfonic acid); TCEP, tris(2-carboxyethyl)phosphine hydrochloride; BME, mercaptoethanol; CM-52, carboxymethyl cellulose; ICP-MS, inductively coupled plasma mass spectrometry; PDB, Protein Data Bank.

## REFERENCES


(1) Ash, D. E., Cox, J. D., and Christianson, D. W. (1999) Arginase: A binuclear manganese metalloenzyme. In *Manganese and Its Role in Biological Processes, Volume 37 of Metal Ions in Biological Systems* (Sigel, A., and Sigel, H., Eds.) pp 407−428, Marcel Dekker, New York.

(2) Christianson, D. W., and Cox, J. D. (1999) Catalysis by metal-activated hydroxide in zinc and manganese metalloenzymes. *Annu. Rev. Biochem. 68*, 33−57.

(3) Christianson, D. W. (2005) Arginase: Structure, mechanism, and physiological role in male and female sexual arousal. *Acc. Chem. Res. 38*, 191−201.

(4) Hirsch-Kolb, H., Kolb, H. J., and Greenberg, D. M. (1971) Nuclear magnetic resonance studies of manganese binding of rat liver arginase. *J. Biol. Chem. 246*, 395−401.

(5) Reczkowski, R. S., and Ash, D. E. (1992) EPR evidence for binuclear manganese(II) centers in rat liver arginase. *J. Am. Chem. Soc. 114*, 10992−10994.

(6) Stone, E. M., Glazer, E. S., Chantranupong, L., Cherukuri, P., Breece, R. M., Tierney, D. L., Curley, S. A., Iverson, B. L., and Georgiou, G. (2010) Replacing $Mn^{2+}$ with $Co^{2+}$ in human arginase I enhances cytotoxicity toward L-arginine auxotrophic cancer cell lines. *ACS Chem. Biol. 5*, 333−342.

(7) Dahlig, E., and Porembska, Z. (1977) Reactivation of the EDTA-treated arginase from rat and calf liver. *Acta Biochim. Pol. 24*, 187−196.

(8) Scolnick, L. R., Kanyo, Z. F., Cavalli, R. C., Ash, D. E., and Christianson, D. W. (1997) Altering the binuclear manganese cluster of arginase diminishes thermostability and catalytic function. *Biochemistry 36*, 10558−10565.

(9) McGee, D. J., Zabaleta, J., Viator, R. J., Testerman, T. L., Ochoa, A. C., and Mendz, G. L. (2004) Purification and characterization of *Helicobacter pylori* arginase, RocF: Unique features among the arginase superfamily. *Eur. J. Biochem. 271*, 1952−1962.

(10) Viator, R. J., Rest, R. F., Hildebrandt, E., and McGee, D. J. (2008) Characterization of *Bacillus anthracis* arginase: Effects of pH, temperature, and cell viability on metal preference. *BMC Biochem. 9*, 15.

(11) Di Costanzo, L., Pique, M. E., and Christianson, D. W. (2007) Crystal structure of human arginase I complexed with thiosemicarbazide reveals an unusual thiocarbonyl $\mu$-sulfide ligand in the binuclear manganese cluster. *J. Am. Chem. Soc. 129*, 6388−6389.

(12) Baggio, R., Elbaum, D., Kanyo, Z. F., Carroll, P. J., Cavalli, R. C., Ash, D. E., and Christianson, D. W. (1997) Inhibition of $Mn^{2+}{}_2$-arginase by borate leads to the design of a transition state analogue inhibitor, 2(*S*)-amino-6-boronohexanoic acid. *J. Am. Chem. Soc. 119*, 8107−8108.

(13) Di Costanzo, L., Sabio, G., Mora, A., Rodriguez, P. C., Ochoa, A. C., Centeno, F., and Christianson, D. W. (2005) Crystal structure of human arginase I at 1.29-Å resolution and exploration of inhibition in the immune response. *Proc. Natl. Acad. Sci. U.S.A. 102*, 13058−13063.

(14) D'Antonio, E. L., and Christianson, D. W. (2011) Crystal structures of complexes with cobalt-reconstituted human arginase I. *Biochemistry 50*, 8018−8027.

(15) Christianson, D. W., and Lipscomb, W. N. (1989) Carboxypeptidase A. *Acc. Chem. Res. 22*, 62−69.

(16) Matthews, B. W. (1988) Structural basis of the action of thermolysin and related zinc peptidases. *Acc. Chem. Res. 21*, 333−340.

(17) Christianson, D. W. (1991) Structural biology of zinc. *Adv. Protein Chem. 42*, 281−355.

(18) Alberts, I. L., Nadassy, K., and Wodak, S. J. (1998) Analysis of zinc binding sites in protein crystal structures. *Protein Sci. 7*, 1700−1716.

(19) Berg, J. M., and Merkle, D. L. (1989) On the metal ion specificity of zinc finger proteins. *J. Am. Chem. Soc. 111*, 3759−3761.

(20) Greenberg, D. M., Bagot, A. E., and Roholt, O. A. (1956) Liver arginase. III. Properties of highly purified arginase. *Arch. Biochem. Biophys. 62*, 446−453.

(21) Tormanen, C. D. (2008) Inhibition of rat and soybean arginase by zinc ion. Abstracts, 236th Annual ACS Meeting, Philadelphia, August 17−21, 2008, BIOL 35.

(22) Issaly, I. M., and Issaly, A. S. (1974) Control of ornithine carbamoyltransferase activity by arginase in *Bacillus subtilis*. *Eur. J. Biochem. 49*, 485−495.

(23) Moreno-Vivian, C., Soler, G., and Castillo, F. (1992) Arginine catabolism in the phototrophic bacterium *Rhodobacter capsulatus* E1F1: Purification and properties of arginase. *Eur. J. Biochem. 204*, 531−537.

(24) Gomez-Ortiz, M., Gomis-Ruth, F. X., Huber, R., and Aviles, F. X. (1997) Inhibition of carboxypeptidase A by excess zinc: Analysis of the structural determinants by X-ray crystallography. *FEBS Lett. 400*, 336−340.

(25) Holland, D. R., Hausrath, A. C., Juers, D., and Matthews, B. W. (1995) Structural analysis of zinc substitutions in the active site of thermolysin. *Protein Sci. 4*, 1955−1965.

(26) Archibald, R. M. (1945) Colorimetric determination of urea. *J. Biol. Chem. 157*, 507−518.

(27) Rüegg, U. T., and Russell, A. S. (1980) A rapid and sensitive assay for arginase. *Anal. Biochem. 102*, 206−212.

(28) Otwinowski, Z., and Minor, W. (1997) Processing of X-ray diffraction data collected in oscillation mode. *Methods Enzymol. 276*, 307−326.

(29) McCoy, A. J., Grosse-Kunstleve, R. W., Storoni, L. C., and Read, R. J. (2005) Likelihood-enhanced fast translation functions. *Acta Crystallogr. D61*, 458−464.

(30) Collaborative Computational Project, Number 4 (1994) The CCP4 suite: Programs for protein crystallography. *Acta Crystallogr. D50*, 760−763.

(31) Brünger, A. T., Adams, P. D., Clore, G. M., Delano, W. L., Gros, P., Grosse-Kunstleve, R. W., Jiang, J. S., Kuszewski, J., Nilges, N., Pannu, N. S., Read, R. J., Rice, L. M., Simonson, T., and Warren, G. L. (1998) Crystallography and NMR system (CNS): A new software system for macromolecular structure determination. *Acta Crystallogr. D54*, 905−921.

(32) Emsley, P., and Cowtan, K. (2004) Coot: Model-building tools for molecular graphics. *Acta Crystallogr. D60*, 2126−2132.

(33) Laskowski, R. A., MacArthur, M. W., Moss, D. S., and Thornton, J. M. (1993) PROCHECK: A program to check the stereochemical quality of protein structures. *J. Appl. Crystallogr. 26*, 283−291.

(34) Kleywegt, G. J., Zou, J. Y., Kjeldgaard, M., and Jones, T. A. (2001) Around O. In *International Tables of Crystallography* (Rossmann, M. G., and Arnold, E., Eds.) pp 353−356, 366−367, Kluwer Academic Publishers, Dordrecht, The Netherlands.

(35) Beale, R. N., and Croft, D. (1961) A sensitive method for the colorimetric determination of urea. *J. Clin. Pathol. 14*, 418−424.

(36) Carrell, C. J., Carrell, H. L., Erlebacher, J., and Glusker, J. P. (1988) Structural aspects of metal ion-carboxylate interactions. *J. Am. Chem. Soc. 110*, 8651−8656.

(37) Cavalli, R. C., Burke, C. J., Soprano, D. R., Kawamoto, S., and Ash, D. E. (1994) Mutagenesis of rat liver arginase expressed in *Escherichia coli*: Role of conserved histidines. *Biochemistry 33*, 10652−10657.

(38) Colleluori, D. M., Reczkowski, R. S., Emig, F. A., Cama, E., Cox, J. D., Scolnick, L. R., Compher, K., Jude, K., Han, S., Viola, R. E., Christianson, D. W., and Ash, D. E. (2005) Probing the role of the hyper-reactive histidine residue of arginase. *Arch. Biochem. Biophys. 444*, 15−26.

(39) Christianson, D. W., and Alexander, R. S. (1989) Carboxylate-histidine-zinc interactions in protein structure and function. *J. Am. Chem. Soc. 111*, 6412−6419.

(40) Daghigh, F., Cavalli, R. C., Soprano, D. R., and Ash, D. E. (1996) Chemical modification and inactivation of rat liver arginase by *N*-bromosuccinimide: Reaction with His141. *Arch. Biochem. Biophys. 327*, 107−112.

(41) Carvajal, N., Olate, J., Salas, M., Uribe, E., López, V., Herrera, P., and Cerpa, J. (1999) Chemical modification and site-directed mutagenesis of human liver arginase: Evidence that the imidazole group of histidine-141 is not involved in substrate binding. *Arch. Biochem. Biophys. 371*, 202−206.

(42) Vockley, J. G., Tabor, D. E., Kern, R. M., Goodman, B. K., Wissmann, P. B., Kang, D. S., Grody, W. W., and Cederbaum, S. D. (1994) Identification of mutations (D128G, H141L) in the liver arginase gene of patients with hyperargininemia. *Hum. Mutat. 4*, 150−154.
(43) Kanyo, Z. F., Scolnick, L. R., Ash, D. E., and Christianson, D. W. (1996) Structure of a unique binuclear manganese cluster in arginase. *Nature 383*, 554−557.